Indoor thermal comfort analysis during dynamic frosting-defrosting process of air source heat pumps

Wei Wang [a, b], Jianyu Ren [a], Yang Tan [a], Zhiwen Luo [c], Wenzhe Wei [a, *], Xinyue Jin [a], Yuying Sun [a], Chunxiao Zhang [d]

[a] Beijing Key Laboratory of Green Built Environment and Energy Efficient Technology, Beijing University of Technology, Beijing 100124, China

[b] College of Mechatronic Engineering, Beijing Polytechnic University, Beijing 100176, China

[c] Welsh School of Architecture, Cardiff University, Cardiff, United Kingdom

[d] Institute of Building Energy and Thermal Science, Henan University of Science and Technology, Luoyang, 471023, China

*Corresponding author, E-mail address: weiwzhe@bjut.edu.cn (W. Wei)

Abstract

During the defrosting operation of air source heat pump (ASHP) and a period thereafter, it stops supplying heating to indoor space. This leads to indoor temperature drop significantly, and further causes thermal discomfort for subjects. To improve the thermal comfort during the frosting-defrosting process of ASHP, two test rigs, one air-water heat pump (AWHP) heating system and one air-air heat pump (AAHP) heating system, were built in an artificial climate chamber. Under the standard frosting condition of 2/1 °C, space heating experiments were conducted to investigate the variations of indoor environment and thermal sensation of subjects during the frosting-defrosting process. Results showed that the indoor temperature declined notably during the defrosting operation for AWHP and AAHP. Specifically, the temperature decreased 2.6-4.6 °C for AWHPs, and 1.4-1.9 °C for AAHPs. Owing to the decrease in indoor temperature and the increase in draught sensation, the thermal sensation of subjects in AWHP-heated rooms and AAHP both decreased significantly. 78.4% subjects in AWHP-heated rooms and 73.5% subjects in AAHP-heated rooms reported a downgrade in thermal sensation after defrosting. Then, the acceptable indoor temperature at the beginning time of defrosting were calculated, and they were respectively 20.74-25.09 °C and 19.91-24.45 °C for the AWHP-heated rooms and AAHP.

Keywords： air source heat pump; frosting; defrosting-induced indoor temperature fluctuation; indoor thermal comfort; acceptable indoor temperature at the beginning time of defrosting

Nomenclatures

T_c	Outdoor coil surface temperature (°C)
T_a	Ambient air temperature (°C)
T	Cumulative continuous heating duration of the ASHPs (min)
T_{in}	Indoor temperature at the start of defrosting (°C)
T_{lowest}	The lowest temperature during defrosting processes (°C)
T_r	The temperature reductions values between T_{in} and T_{lowest} (°C)
RH	Relative humidity (%)
$RH_{highest}$	The highest relative humidity during defrosting processes (%)
RH_{in}	Indoor relative humidity at the start of defrosting (%)
RH_r	Relative humidity fluctuations in the room (%)

Abbreviation

ASHP	Air source heat pump
COP	Coefficient of performance
RCD	Reverse-cycle defrosting
PMV	Predicted mean vote
PPD	Predicted percentage dissatisfied
AWHP	Air-water heat pump
AAHP	Air-air heat pump
TSV	Thermal sensation vote

1 Introduction

With the proposal of dual-carbon goal [1], countries worldwide have accelerated the utilization of energy-saving technologies [2-4]. As an energy-efficient and high-performance heating technology [5, 6], air source heat pumps (ASHPs) are capable of converting low-grade thermal energy from ambient air into usable heat [7, 8], while offering the advantages of low cost and ease of installation [9, 10]. In recent years, ASHPs have been extensively adopted for space heating in buildings across China. However, in practical applications, ASHPs frequently encounter frosting problem on the surface of the outdoor heat exchanger.

During space heating, frosting accumulates on the surface of the outdoor coil when its temperature simultaneously falls below the dew point of the ambient air and the freezing point [11]. The accumulation of frost increases the heat transfer resistance between the outdoor coil and the surrounding air, while simultaneously reduces the airflow rate through the coil [12, 13]. These effects can lead to a reduction of more than 30% in the heating capacity and coefficient of performance (COP) of the ASHP [14, 15], and may even result in physical damage to the equipment.

To maintain the reliable operation of ASHPs, periodic defrosting is unavoidable [16]. Among the various defrosting strategies, the reverse-cycle defrosting (RCD) method is the most widely adopted one in ASHPs [17]. In the RCD method, the four-way valve is switched to convert the outdoor coil into a condenser, directly discharging the high-temperature refrigerant from compressor into the outdoor coil. As the refrigerant cools and condenses within the outdoor coil, it releases heat to melt the accumulated frost layer. Meanwhile, the indoor unit operates as an evaporator. Consequently, during reverse-cycle defrosting, the ASHP suspends space heating and may even absorb heat from the indoor environment [11]. This process results in significant fluctuations in the indoor thermal environment following defrosting, further compromising subjects' thermal comfort [18, 19]. Therefore, frosting and defrosting are critical factors influencing the overall heating performance of ASHPs.

Regarding the frosting and defrosting challenges in ASHPs, previous studies have primarily concentrated on frosting mechanisms [20-22], frosting patterns [23-25] and defrosting efficiency [26-28], with the overarching goal of improving indoor thermal comfort by enhancing defrosting accuracy and shortening defrosting duration. To improve defrosting accuracy, Wang et al. [29] proposed the optimal defrosting initiation time theory, which minimizes heating capacity losses during the frosting–defrosting cycle by initiating defrosting at the optimal moment. Building on this theory, Li et al. [30] developed an image recognition–based defrosting method that enables precise defrosting control by using characteristic parameters to detect frosting in real-world applications. Tang et al. [31] proposed a defrosting control strategy based on outdoor temperature, fan current, and outdoor coil temperature, exploiting variations in fan current during the frosting process as a control signal. Compared with the conventional time–temperature control method, this approach reduced the defrosting frequency from 0.93 time to 0.56 time and extended the average heating duration by 66.25%. In parallel, considerable research efforts have been devoted to reducing defrosting duration. Wei et al. [32] employed vapor injection technology to increase refrigerant mass flow in quasi–two-stage compression systems, thereby shortening the defrosting period. Their results indicated that, with vapor injection technology, the defrosting duration of low-temperature ASHPs could be reduced by up to 20.61%. The results indicate that this technology can effectively enhance the heat transfer rate of the ASHP. Qu et al. [33] introduced a thermal energy storage (TES)–based RCD method, which shortened defrosting duration by 71.4%–80.5% compared with the standard hot-gas bypass defrosting method. Liu et al. [34] developed performance maps for variable-frequency ASHPs by combining different compressor speeds and outdoor fan flow rates to guide defrosting operations, resulting in a 157.68% increase in heating duration. Collectively, these researches have mitigated the adverse impact of the frosting–defrosting process on fluctuations in the indoor thermal environment, thereby improving indoor thermal comfort.

From the above review, it is evident that substantial research efforts have been devoted to improving indoor thermal comfort during the defrosting process. However, direct investigations focusing specifically on indoor thermal comfort remain limited in the existing literatures. Qu et al. [35] examined indoor thermal comfort during the actual defrosting process by applying a TES-based RCD method. In their study, predicted mean vote (PMV) and predicted percentage dissatisfied (PPD) were employed as indicators of indoor thermal comfort, with the thermal environment considered acceptable when PPD < 10% or −0.5 < PMV < 0.5. Their results demonstrated that, under the TES-based RCD method, the duration of the comfort range—based on indoor PMV values—increased from 16 min to 46 min compared to the standard mode. Mao et al. [36] investigated the effects of ASHP operation before and after defrosting on human thermal comfort during sleep, reporting that the PMV value dropped to a minimum of −0.83 during defrosting, with sensations of coolness and slight coolness persisting for approximately 45.4 min. However, indoor temperature and humidity vary rapidly during the frosting–defrosting process, whereas the PMV–PPD model is formulated under steady-state conditions. Moreover, the aforementioned studies were conducted in actual heating buildings, where uncontrollable outdoor environmental conditions preclude repeated testing, thereby making it harder to extrapolate their results to future studies. Consequently, the variation characteristics of indoor thermal comfort throughout the frosting–defrosting process remain insufficiently understood, which significantly constrains the optimization of defrosting control strategies. This underscores the urgent need for a systematic and comprehensive investigation into the effects of defrosting operations on the indoor thermal environment and human thermal comfort.

To address the above issues, a representative rural residential building from the Yangtze River Basin of China was constructed within an artificial climate chamber and equipped with an air-water heat pump (AWHP) and an air-air heat pump (AAHP) test rigs for space heating experiments. By establishing a stable frosting environment in the artificial climate chamber, frosting and defrosting experiments were conducted under different indoor set temperatures. Meanwhile, the indoor thermal comfort during the frosting-defrosting process was investigated through collecting subjects' thermal sensation feedback via questionnaires. The main originalities of the present work are as follows: (1) revealing the variation patterns of the indoor thermal environment during the frosting-defrosting process quantitatively; (2) exploring the impact of defrosting operation on indoor dynamic thermal comfort through the questionnaire survey; and (3) proposing the acceptable indoor temperature ranges at the beginning of defrosting for both AWHP and AAHP systems, to improve indoor thermal comfort during frosting-defrosting process. These findings provide a foundation for optimizing the indoor thermal environment during ASHP defrosting and contribute to enhancing the indoor thermal comfort in rooms heated by ASHPs.

2 Experimentation

2.1 The artificial climate chamber

To investigate the indoor thermal comfort during the frosting-defrosting process, the frosting and defrosting experiments of ASHPs were conducted in an artificial climate chamber. This chamber is a specialized laboratory designed to study indoor thermal comfort and thermal environments by simulating specific outdoor conditions. It was constructed following building envelope standards for the Hot Summer and Cold Winter climatic region of China. The materials and sizes of the building envelope, including walls, windows and floor, are widely employed in the Yangtze River Basin. Consequently, the thermal inertia of the internal room is same with those real buildings.As shown in Fig. 1(a), the chamber consists of an external chamber and an internal chamber. The external chamber creates a stable frosting environment and houses the outdoor unit of the ASHP. The internal chamber is a two-story building used for conducting thermal comfort experiments during the ASHP frosting and defrosting process. Its envelope structure is based on typical rural residential buildings from the middle and lower reaches of the Yangtze River, China. The plans of the first and second floors of the internal chamber are shown in Fig. 1(b) and Fig. 1(c), respectively, with each floor containing three rooms. The three rooms on the second floor, with areas of 62.08 m^2, 20.99 m^2, and 38.92 m^2, are all heated by an AWHP. On the first story, an AAHP was adopted for space heating. Unlike the multi-indoor fan coils structure in AWHP, one AAHP can supply heat for only one room because its single indoor heat exchanger. Consequently, the AAHP only supplied heat for Room 4 (15.57 m^2). Therefore, Rooms 1–4 were selected for the ASHP thermal comfort experiments in this work.

The heating terminals for AAHP and AWHP were all fan coils, and they are suspended from the ceiling. In each room, there is only one fan coil. All the fan coils were installed near the middle point of the shorter wall in each room. The distance between their lower surfaces and floor is 2.7 m, and the distance between their inlets and the wall is 0.2 m.

(a)Three-dimensional diagram of artificial climate chamber

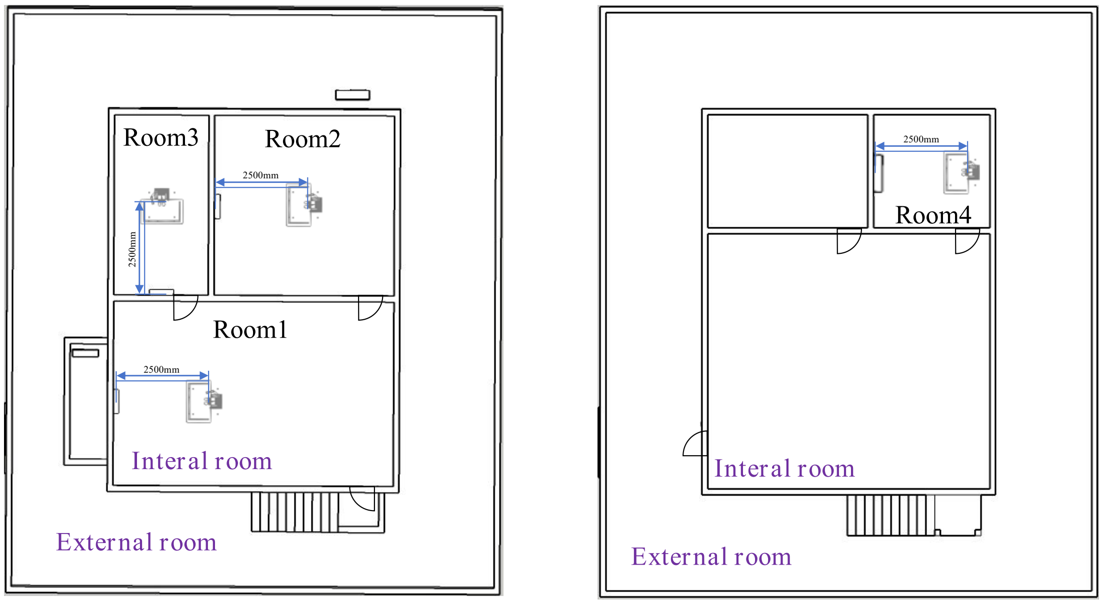

(b) second floor (c) first floor

Fig. 1 Detailed information of the artificial climate chamber

2.2 The experimental air source heat pumps

Based on the type of flow medium in the condenser, ASHPs can be classified into two main types: AAHPs and AWHPs. In AWHP heat system, there is a substantial amount of heat stored in the circulating water at the beginning of defrosting operation, which can be utilized for space heating during the defrosting process. Consequently, the indoor fan coils are kept operating throughout the defrosting process. In contrast, to prevent absorbing heat from the indoor environment, the indoor fan coils of AAHPs are generally turned off during defrosting [37]. Thus, AAHPs do not supply heat to indoors and may even induce heat loss through natural convection. Therefore, the operational states of the indoor fan coils of the two types of ASHPs are opposite during defrosting, which has led researchers to generally think that the indoor thermal comfort differs between them during their frosting and defrosting process.

To investigate the variation trends of the indoor temperature and relative humidity during the frosting-defrosting process of ASHPs, an AWHP and an AAHP were employed, with their schematic diagrams shown in Figs. 2(a) and 2(b), respectively. The AWHP comprises an outdoor unit and three indoor fan coils, supplying heat to Rooms 1-3 on the second floor of the internal chamber. It uses R410A as the refrigerant, with a rated heating capacity of 18 kW and a rated COP of 3.1. The AAHP consists of one outdoor unit and one indoor unit, supplying heat to Room 4 on the first floor of the internal chamber. It employs R32 as the refrigerant, with a rated heating capacity of 3.5 kW and a rated COP of 3.3. As the refrigerant types have little effect on the defrosting performance of ASHP [38], the refrigerant difference of the two ASHPs will not affect the experimental results in this work. The AWHP and AAHP have a 3 kW and 1 kW backup heater, respectively. Since the experimental environment was not an extreme one, both the two backup heaters were not turned on during the experimental process. The detailed specifications of the outdoor units for both ASHPs are shown in Table 1. To make the water capacity in AWHP heating system similar to those in practical projects, a small water tank was adopted and connected to the circulation water system, and the total water capacity was 65 L.

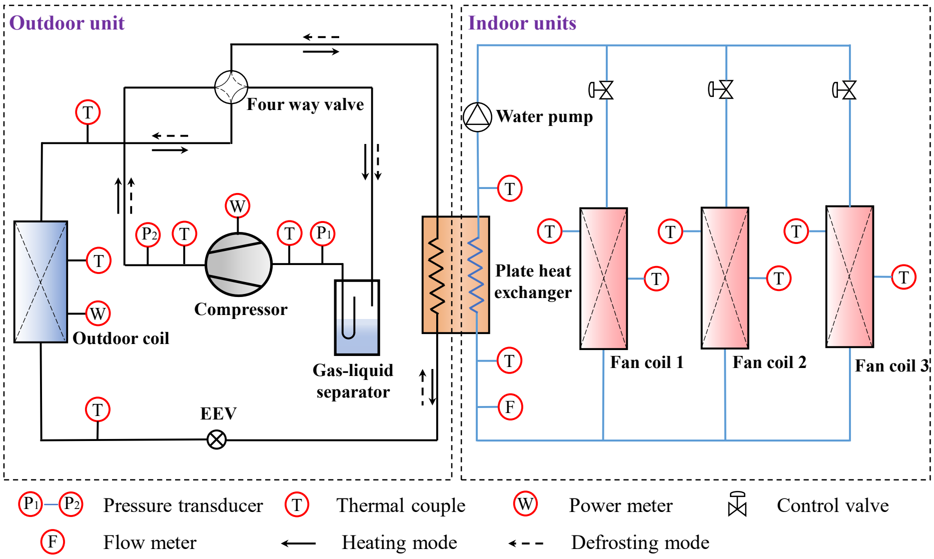

(a) air-water heat pump

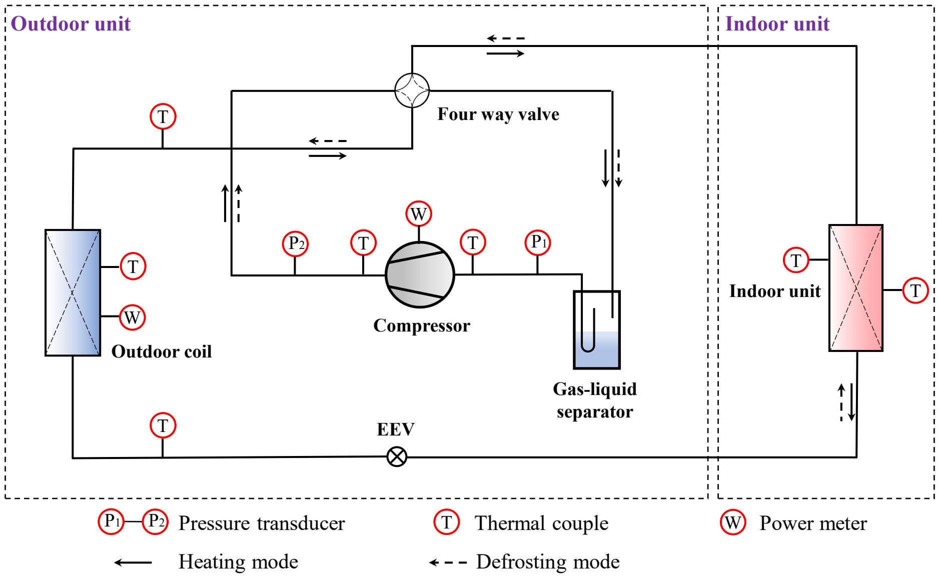

(b) air-air heat pump

Fig. 2 Schematic diagrams of the experimental ASHPs

For the both ASHPs, the RCD method were adopted, with control logic based on the *ΔT*–*T* strategy. *ΔT* is the difference between the outdoor ambient temperature (T_a) and the outdoor coil surface temperature (T_c) of the outdoor coil, while the *T* represents the cumulative operation duration of the ASHPs. Under frosting conditions, *ΔT* increases as the frost layer on the outdoor coil thickens. When *ΔT* exceeds the set threshold of 7.0 °C and *T* exceeds 40 min, the defrosting operation initiates. Once the above two criteria, i.e 7.0 °C and 40 min, are met, the evaporator and condenser are reversed via switching the four-way valve, allowing high-temperature refrigerant discharged from the compressor to flow through the outdoor coil and melt the frost layer. The indoor fan coil of the AWHP remains running and continues to supply heat to the indoor space, while the indoor fan coil of AAHP is turned off. Defrosting terminates when the T_c reaches 20 °C, and then the four-way valve is switched again to resume heating. To decrease the pressure differential across the four-way valve during switching, the AWHP is shut down for 2 min before each switching operation. For AAHP, as the pressure differential between condenser and evaporator is far smaller, it shuts down for only 1 min before each switching. After resuming heating, the surface temperature of the indoor fan coil of AAHP remains relatively low. To avoid blowing cold wind after defrosting, its indoor fan begins to run only after the coil temperature reaches 35 °C [12, 37].

In the USA, the EU, and China, the frosting performance of ASHPs are all conducted under the environmental condition of 2/1 °C (dry-bulb/wet-bulb temperature) [38], according to the Chinese National Standard, *Low Ambient Temperature Air Source Heat Pump (Water Chilling) Packages* (GB/T 25127-2020) and the American National Standard [39], *Performance Rating of Water-Chilling and Heat Pump Water-Heating Packages Using the Vapor Compression Cycle* (ANSI/AHRI 550/590–2023) [40]. the frosting of ASHPs under this condition is typical. To ensure the universality and comparability of experimental results, the outdoor environmental parameters in this study (i.e., the conditions in the external chamber of the artificial climate chamber) were also set at 2/1 °C.

Table 1 Specifications of the outdoor units

Parameters	Values/Details	
	air-water heat pump	air-air heat pump
Refrigerant	R410A	R32
Rated heating capacity (kW)	18	3.5
Rated COP	3.1	3.3
Rated condition	7/6 °C	7/6 °C
Compressor type	scroll	rotor
Compressor speed (r/s)	40-100	20-100
Type of outdoor coil	finned tube	finned tube
Tube type	inner grooved tube	inner grooved tube
Tube material	copper	copper
Fin material	aluminum	aluminum

During the winter in hot-summer and cold-winter climatic regions of China, the indoor temperature is typically maintained at 22-24 °C when ASHPs are used for space heating. To realistically capture the impact of frosting-defrosting on the indoor thermal environment, the set temperatures for the three rooms heated by the AWHP were 22 °C, 23 °C, and 24 °C, respectively, while the set temperature for the room heated by the AAHP was 23 °C. During the stable heating prosses, the allowable indoor temperature fluctuation, defined as the temperature return difference, was ±3 °C for all the four rooms. Accordingly, the actual indoor temperatures for the three AWHP-heated rooms were 22 ± 3 °C, 23 ± 3 °C, and 24 ± 3 °C, while the AAHP-heated room room was maintained at 23 ± 3 °C. Detailed settings for both the outdoor and indoor environments are summarized in Table 2.

As the compressor speed and fan frequency both have great effect on the frosting rate, they were both fixed during the experiments to obtain the controllable and repeatable experimental results. In preliminary tests, it was observed that when the AWHP compressor operated at 70 Hz and the outdoor fan operated at 1750 rpm, the heating capacity approximately matched the building heating load. Consequently, these values were adopted for the AWHP during the experiment. Using the same approach for the AAHP, the compressor and outdoor fan speeds were set at 50 Hz and 450 rpm, respectively. The detailed settings for compressor and outdoor fan speeds are shown in Table 2.

Table 2 Experimental setup for ASHP heating

Types	Compressor rotate speed (Hz)	Outdoor fan speed (rpm)	Outdoor environmental condition (°C)	Indoor temperature setpoint (°C)
Air-water heat pump	70	1750	2/1	Room 1: 24 Room 2: 23 Room 3: 22
Air-air heat pump	50	450		Room 4: 23

2.3 The data acquisition system

To collect the required data, monitoring points were arranged on both the ASHP units and indoors, with detailed specifications listed in Table 3. The specific arrangements are as follows:

(1) Monitoring of ASHP operating parameters

Two pressure transducers were installed on the compressor suction and discharge pipelines to monitor suction and discharge pressures. An intelligent electric meter has been installed to record the instantaneous input power of the outdoor unit. Five temperature sensors were installed at key points along the refrigerant circuit in outdoor unit to monitor the refrigerant temperature, as illustrated in Fig. 3. Besides, for AWHP, two temperature sensors were mounted on the water supply and return pipelines to measure water temperature variations. An electromagnetic flowmeter was installed on the main water supply pipe to measure the total water flow rate.

(2) Monitoring of the outdoor environment

A temperature & humidity sensor was positioned near the outdoor unit to monitor outdoor air temperature and relative humidity.

(3) Monitoring of the indoor environment

Numerous thermocouples and temperature-humidity sensors were installed indoors. In addition, a black globe thermometer and an anemometer were deployed to measure indoor mean radiant temperature and air velocity, respectively. The specific arrangements of the sensors are as follows:

1) Indoor temperature measurement

The plane distribution of indoor temperature measuring points is shown in Figs. 3(a) and 3(c). Each measuring point was equipped with a vertical measuring line. In AWHP-heated rooms, temperature sensors were arranged at heights of 0.3 m, 0.8 m, 1.3 m, 1.8 m, and 2.3 m along each vertical line. The same height arrangement was used in AAHP-heated rooms. Additionally, three thermocouples were installed at both the air inlet and outlet of the AAHP to measure the inlet and outlet air temperatures. In total, 270 (9×6×5), 150 (6×5×5), and 90 (6×3×5) thermocouples were installed in the three AWHP-heated rooms, respectively, while 216 (7×6×5+3×2) thermocouples were installed in the AAHP-heated room.

2) Indoor humidity measurement

The plane distribution of indoor humidity measuring points is shown in Figs. 3(b) and 3(d). Humidity sensors were arranged according to *the Standard of Test Methods for Thermal Environment of Buildings (JGJ/T 347-2014)*. In the larger AWHP-heated rooms (Room 1), the two diagonals were selected, and five measuring points were placed at the intersection and quarter points of the diagonals. In the two smaller AWHP-heated rooms, one diagonal was selected per room, with two and three measuring points placed at the trisection and quarter points, respectively. In Room 4, a single measuring point was placed at the intersection of the diagonals. At present, since the ASHPs don't have the function of adjusting indoor humidity at present, the humidity variations during frosting-defrosting cycles cannot be solved without additional humidification device. Consequently, the humidity variation was not main concern of this work, and all the relative humidity sensors were installed at the height of 0.6 m without considering its vertical variation.

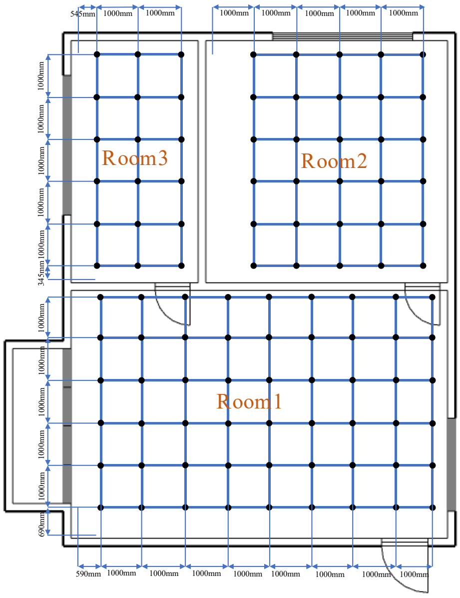

(a)Thermocouples in AWHP-heated rooms

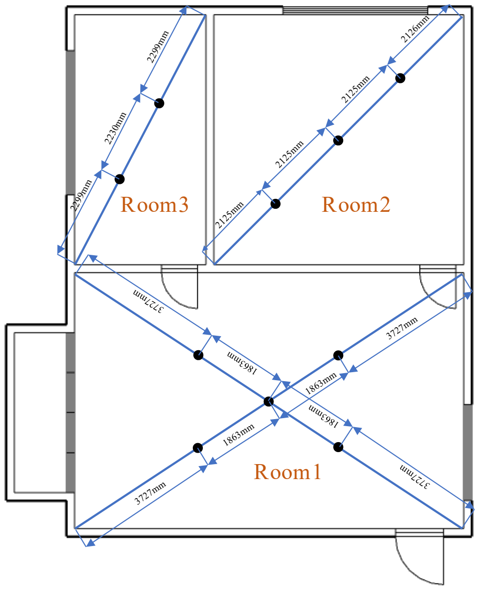

(b) Relative humidity sensors in AWHP-heated rooms

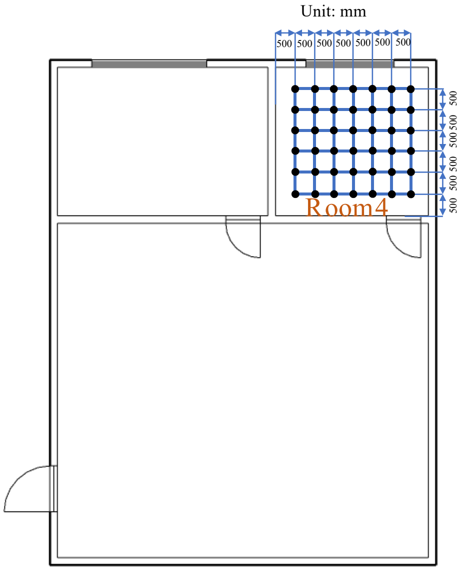

(c)Thermocouples in AAHP-heated room

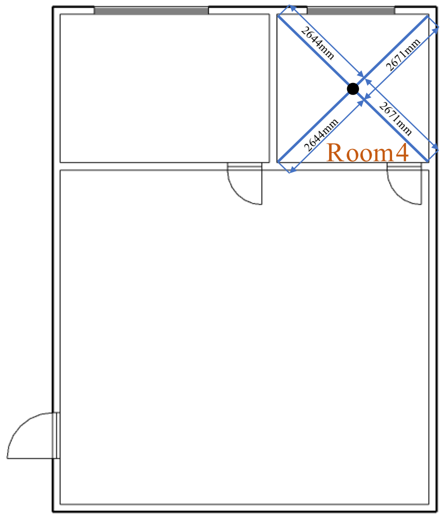

(d) Relative humidity sensors in AAHP-heated room

Fig. 3 Floor plan of thermocouples and relative humidity sensors layout in the rooms

Table 3 Detailed specifications of measuring instruments

Name	Measuring range	Error	Number
Thermocouple	-20–100 °C	± 0.1 °C	738
Temperature & humidity sensor	Temp: 0–50 °C RH: 0–100 %	±0.15 °C ±3 %	33
Electromagnetic flow meter	0.1–3.0 m^3 /h	0.5% FS	1
Power meter	0–6.6 kW	0.25% FS	4
Black bulb temperature	0–80 °C	±0.1 °C	13
Hot-wire anemometer	0–30 m/s	±0.5 %	31
Pressure transducer	0–3.0 MPa	0.3% FS	4

2.4 Experimental procedure

To assess thermal comfort during the frosting and defrosting processes, a total of 34 subjects, including 27 males and 7 females, were recruited to complete subjective questionnaires. All subjects were young adults in good health, and their basic characteristics are summarized in Table 4. All subjects maintained a normal diet and regular work-rest schedule within 24 hours prior to the experiment. During the experiments, each subject sequentially entered the four rooms to complete the questionnaire, with one subject per room tested simultaneously. They were seated 2.5 m directly in front of the air supply outlets, as displayed in Fig. 1. One subject entered the room alone for each experiment. The testing sequence for the subjects adopted a completely randomized design, where the order in which each subject experienced the two systems was randomly determined. Additionally, to avoid learning effects, a rest period of at least 30 min was set between the two tests.

It is worth noting that the experiments in this work were conducted in the lab of an air-conditioner manufacture, and the volunteers who are not employees of this company are not allowed to enter the lab. Consequently, the subjects of this experiment are composed of the members of our team participating in the experiment and some employees of the manufacturer. Besides, the employees working this lab are almost all young ones. As the proportion of the older employees is very low, the age distribution of the subjects is unreasonable if they we invited to attend this experiment. Therefore, only young ones working in this lab is invited to participate as subjects in this experiment, as shown in Table 4.

Table 4 Basic information of the subjects

	Age(yr)	Height(m)	Weight(kg)	BMI(kg/m^2)
Males	25±4	1.73±0.05	63±4.10	21.04±2.70
Females	25±1	1.6±0.02	53±3.80	20.7±2.00

Before conducting the experiments in this work, preliminary experiments were conducted to regulate the ASHP heating capacity. After each ASHP was turned on, its heating capacity was adjusted by modifying the compressor speed and outdoor fan frequency. Once the indoor temperature of each room stabilized at the target setpoint, it was assumed that the heating capacity of the ASHP matched the building heating load. After analysis, it was found that when the AWHP operated at a compressor speed of 70 rps and an outdoor fan frequency of 1750 rpm, its heating capacity approximately matched the building heating load. Similarly, for the AAHP, a compressor speed of 50 rps and an outdoor fan frequency of 450 rpm were found to meet the required heating load. During the experiments, the compressor frequency and fan speed were set according to these values, ensuring stable operation of the ASHP. Simultaneously, the subjects were guided in their preparation for the experiment. Once preparations were complete, the experiment commenced, with the detailed procedure illustrated in Fig. 4.

The steps for the subjects during the experiment were as follows:

(1) Change their clothes to specific ones with a thermal resistance of 1.0 clo.

(2) Sit quietly in the preparatory room for approximately 30 min to stabilize and adapt their physical and mental conditions before the experiment.

(3) As shown in Fig. 5, subjects entered the heated rooms, sat quietly to complete the questionnaire. Each subject entered the room 30 min after the end of the former defrosting operation. The first questionnaire was completed after sitting quietly for 5 min. The second questionnaire was completed at the

start of defrosting. For AWHP-heated rooms, the third questionnaire was completed at the end of defrosting, while for the AAHP-heated rooms, it was completed when the indoor fan resumed operation after defrosting. The fourth questionnaire was completed 10 min after the end of the defrosting operation. Apart from the above four questionnaires, subjects can fill additional ones once their thermal sensation changed during the experimental process.

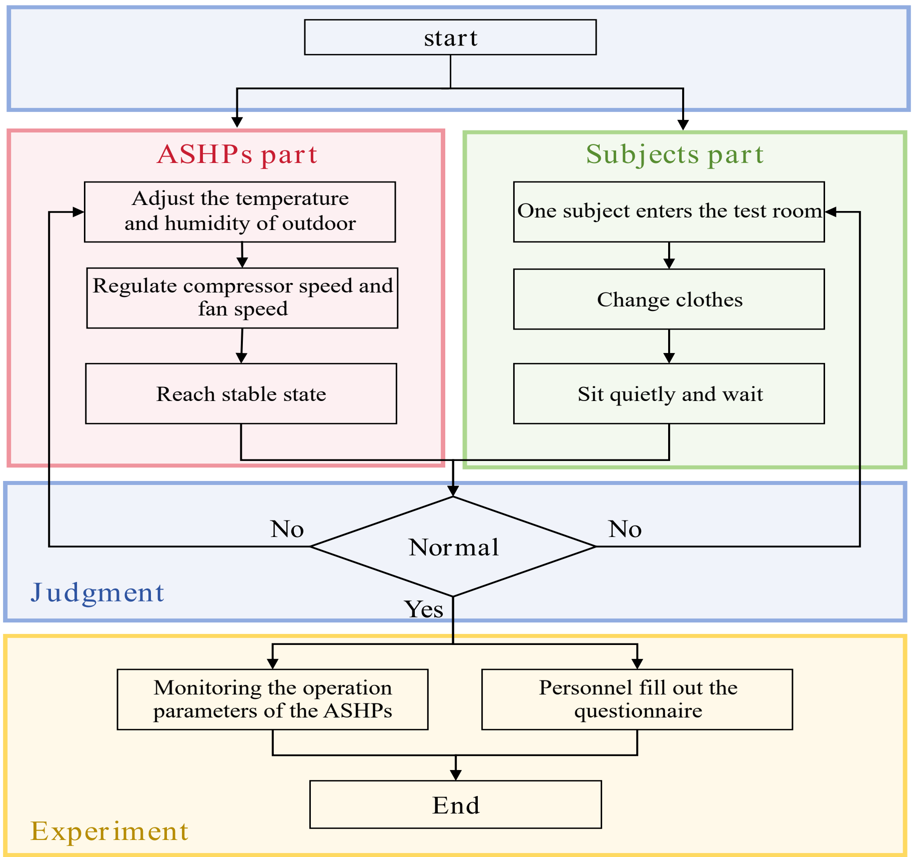

Fig.4 Experimental process for ASHPs and subjects

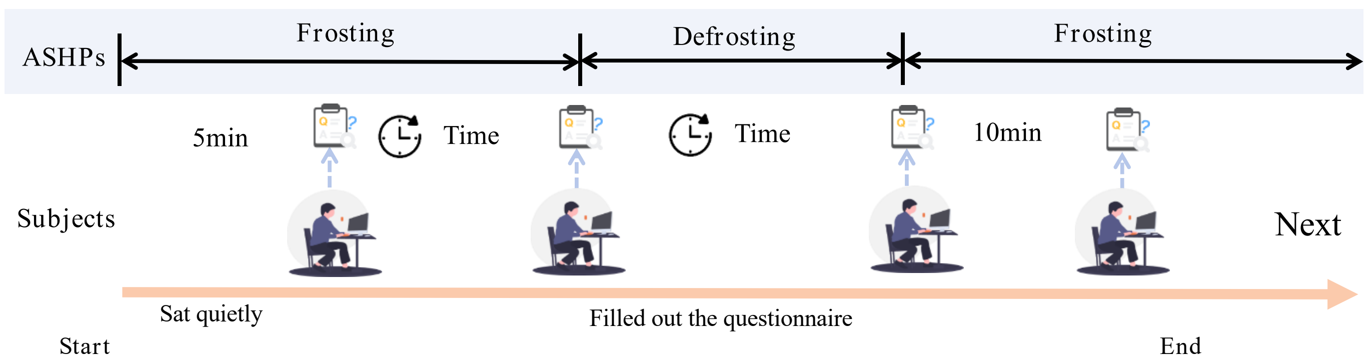

Fig.5 Experimental process for subjects

The questionnaire comprised the following three aspects:

(1) subjects' basic information: including name and completion time;

(2) Subjective thermal comfort: including thermal sensation, draft sensation, and thermal acceptability;

(3) Subjective preferences: including thermal expectation, humidity expectation, draught sensation expectation, and overall body satisfaction.

The evaluation scales referred to ASHRAE 55 [41], developed by the American Society of Heating, Refrigerating, and Air-Conditioning Engineers (ASHRAE), and ISO 7730 [42], developed by the International Organization for Standardization (ISO). A total of 589 valid questionnaires were obtained in this experiment.

Table 5 Thermal sensation scale

Thermal sensation	Hot	Warm	Slightly warm	Neutral	Slightly cool	Cool	Cold
value	+3	+2	+1	0	-1	-2	-3

3 Results and discussion

3.1 Variations of indoor thermal environment

Fig. 6 illustrates the variations in heating capacity of the AWHP and AAHP during three frosting-defrosting processes. For the AWHP, the frosting durations in the three experimental groups were 47.5 min, 46.4 min, and 44.9 min, respectively, while the corresponding defrosting durations were 2.0 min, 2.9 min, and 2.4 min. Considering that the outdoor unit was shut down for 2 min both before and after each frosting-defrosting process, the total durations of the three groups were 53.5 min, 53.3 min, and 51.3 min, respectively. After each defrosting cycle, the heating capacity recovered rapidly and then stabilized at approximately 10 kW, with steady-state values of 10.03 kW, 10.01 kW, and 9.92 kW across the three groups of experiments. During the frosting process, the heating capacity of the AWHP declined gradually, at the moment of defrosting starting, the heating capacities had decreased to 9.68 kW, 9.58 kW, and 9.03 kW, respectively. The compressor was shut down for 2 min before each four-way valve switching, causing the heating capacity decrease rapidly to zero. After the four-way valve switching, the outdoor coils become condenser and refrigerant released heat to the frost layer, making the frost on outdoor coils melted. At the 50.5 min, 102.7 min, and 154.4 min, the heat absorption values reached the maximum, and they were 21.7 kW, 20.4 kW, and 22.0 kW, respectively. When the defrosting was end, the compressor was shut down for 2 min again, during which the heating capacity remained at zero. After the second four-way valve switching, the AWHP recovered to heating mode, and its heating capacity increased rapidly.

For the AAHP, the frosting durations in the three experimental groups were 46.6 min, 47.8 min, and 45.3 min, respectively, with its defrosting durations of 4.1 min, 4.1 min, and 5.4 min. Considering that the outdoor unit was shut down for 1 min both before and after each defrosting operation, the total durations for the three groups were 52.7 min, 53.9 min, and 52.7 min, respectively. After recovery, the heating capacities stabilized at 2.60 kW, 2.60 kW, and 2.58 kW. Before starting defrosting operation, the heating capacities decreased to 2.44 kW, 2.32 kW, and 2.12 kW, respectively. During the defrosting process and the shutdown periods before and after defrosting, the heating capacity dropped to zero due to the interruption of indoor fan operation.

For the AAHP, the frosting durations in the three experimental groups were 46.6 min, 47.8 min, and 45.3 min, respectively, with its defrosting durations of 4.1 min, 4.1 min, and 5.4 min. Considering that the outdoor unit was shut down for 1 min both before and after each defrosting operation, the total durations for the three groups were 52.7 min, 53.9 min, and 52.7 min, respectively. After recovery, the heating capacities stabilized at 2.60 kW, 2.60 kW, and 2.58 kW. Before starting defrosting operation, the heating capacities decreased to 2.44 kW, 2.32 kW, and 2.12 kW, respectively. During the defrosting process and the

shutdown periods before and after defrosting, the heating capacity dropped to zero due to the interruption of indoor fan operation.

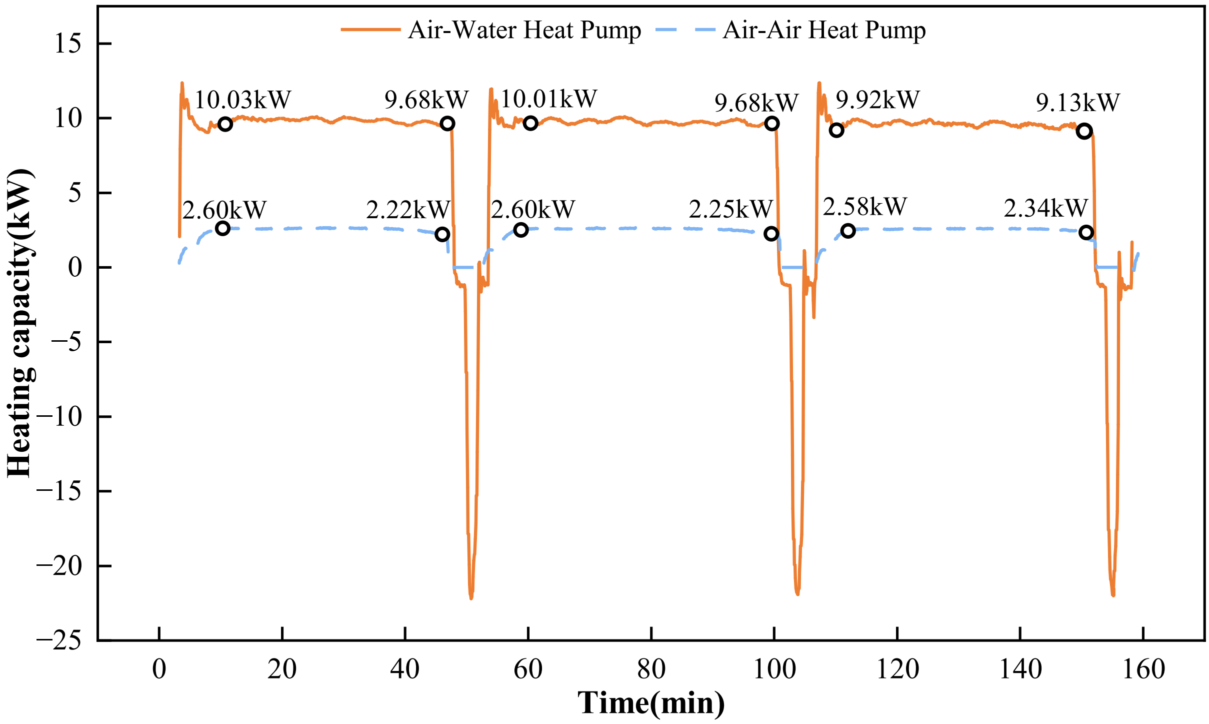

Fig.6 Variation of heating capacity during frosting-defrosting process for AWHP and AAHP

Fig. 7(a) presents the variations in indoor temperature and relative humidity in the rooms heated by the AWHP during three frosting-defrosting processes. During the defrosting process, the refrigerant of outdoor units absorbed heat from the circulating water and led to the drop in indoor temperature. The temperature reduction values (T_r) could be calculated based on the indoor temperature (T_{in}) at the start of defrosting and the lowest temperature (T_{lowest}) after each defrosting, as displayed in Eq. (1).

$$T_r = T_{in} - T_{lowest} \tag{1}$$

The indoor temperature drops during the three groups of experiments were calculated as shown in Table 6, and it was ranged from 2.6 to 4.6 °C, with the maximum reduction value occurring during the first defrosting event in Room 2. After the defrosting process, the indoor temperature increased gradually. Although the AWHP exhibited a relatively short defrosting duration (2.5-2.9 min), it would require as long as 12.6-17.1 min to recover the indoor temperature to the value before defrosting. In contrast, the indoor relative humidity rose sharply during defrosting. By adopting Eq. (2), the rising values could be calculated, and the results were 4.7%–8.8% as expressed in Table 6. Such significant and prolonged variations in temperature and relative humidity inevitably resulted in a marked decline in indoor thermal comfort.

$$RH_r = RH_{highest} - RH_{in} \tag{2}$$

Fig. 7(b) illustrated the indoor temperature and relative humidity variations in the rooms heated by the AAHP. The reduction range of indoor temperature during the three groups of experiments was 1.4-1.9 °C, as shown in Table 6. Meanwhile, the rising range of relative humidity was 4.1–4.4%, as presented in Table 6. Compared to those in AWHP-heated rooms, the fluctuation range in indoor temperature and relative humidity caused by AAHP defrosting were substantially smaller.

Table 6 Reduction values of indoor temperature and increase values of indoor humidity caused by defrosting

Item		1st defrosting	2nd defrosting	3rd defrosting	Average value
Room 1	T_r (°C)	3.5	2.6	3.0	2.9
	RH_r (%)	8.8	5.7	6.1	6.9
Room 2	T_r (°C)	4.6	3.7	4.1	4.1
	RH_r (%)	7.3	4.7	5.0	5.7
Room 3	T_r (°C)	3.7	3.1	3.8	3.5
	RH_r (%)	8.5	6.6	5.6	6.9
Room 4	T_r (°C)	1.4	1.7	1.9	1.7
	RH_r (%)	4.4	4.1	4.4	4.3

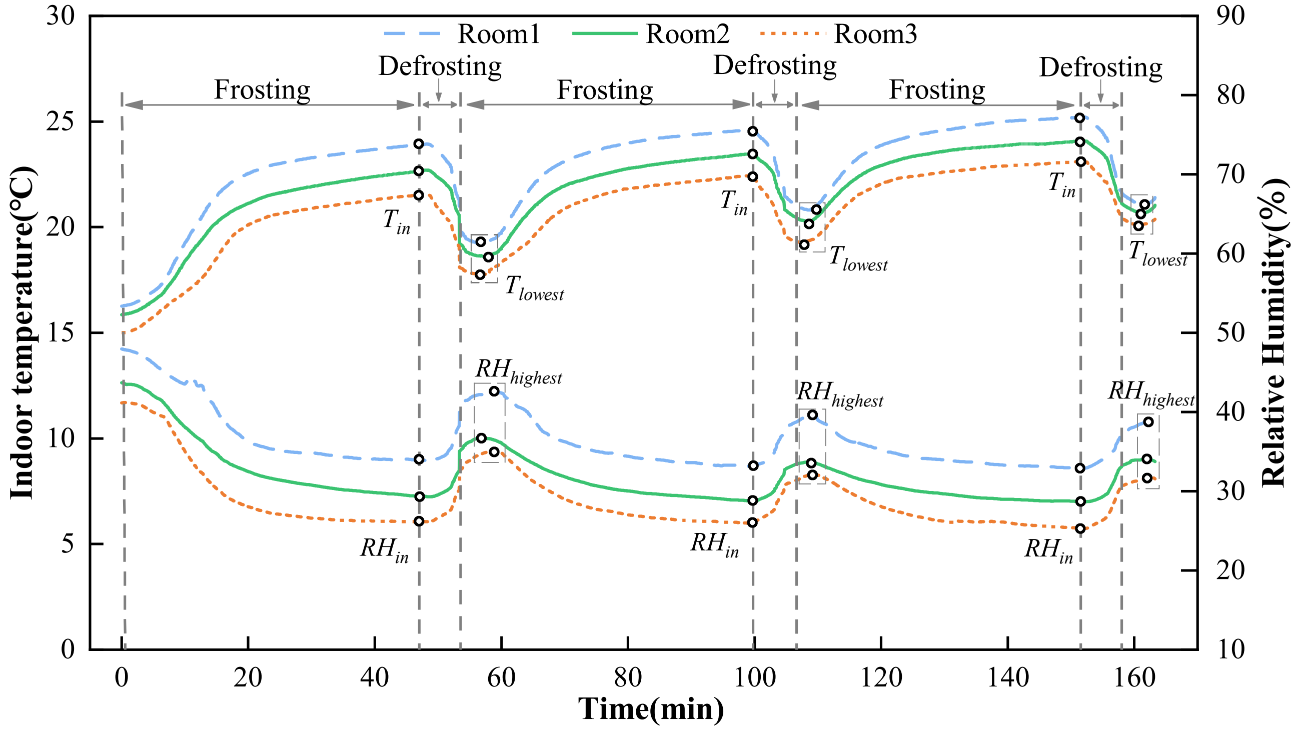

(a) Indoor temperature and relative humidity during experimental processes of AWHP heating

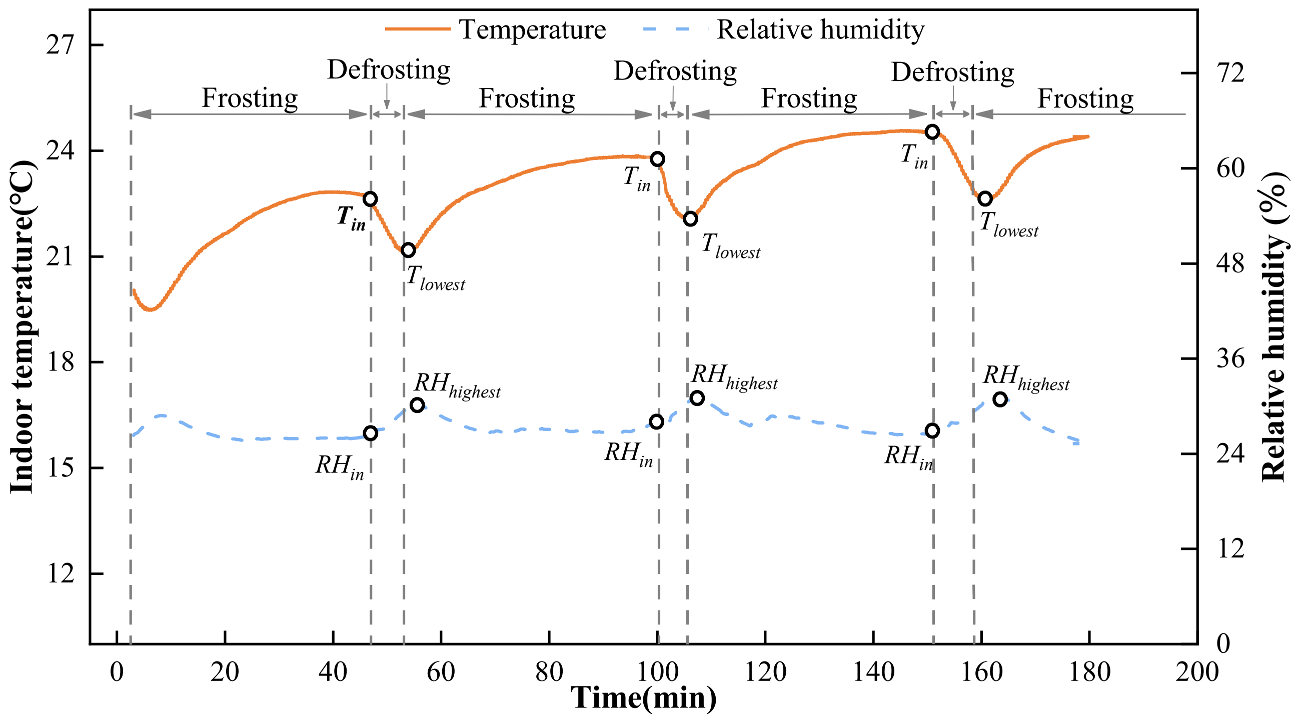

(b)Indoor temperature and relative humidity during experimental processes of AAHP heating

Fig.7 Variations of indoor temperature and relative humidity during experimental processes

3.2 Subjective thermal sensation for subjects

Fig. 8 illustrates the changes in draught sensation vote in rooms heated by AWHP and AAHP before and after the defrosting operation. For the AWHP, its indoor fan coils continued to operate during the defrosting process, causing both the indoor air and the refrigerant to absorb heat from the circulating water. Consequently, the water temperature drops markedly, further leading to a clear increase in indoor draught sensation. Specifically, 41.2% and 22.5% of the subjects reported an increase of one and two levels, respectively.

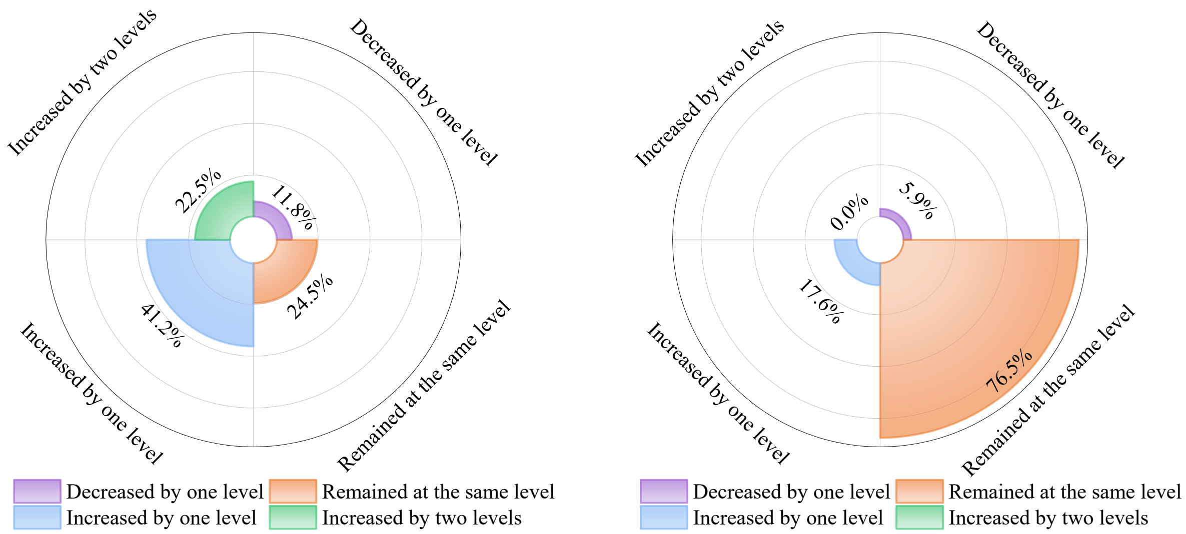

(a) Air-water heat pump (b) Air-air heat pump

Fig.8 Changes in draught sensation after ASHP defrosting

For the AAHP, the indoor fan was turned off during defrosting process, and activated only when the coil temperature increased to 35 °C after defrosting as expressed in Section 2.2. Besides, the temperature drop in the AAHP-heated room after defrosting was smaller, as displayed in Fig. 7. The above two factors ensured a high enough supply air temperature after defrosting. As a result, only 17.6% of the subjects perceived an increase of one level in draught sensation, and none reported a two-level increase. Overall, the proportions of subjects who perceived stronger draught sensation after defrosting were 63.7% in AWHP-heated rooms and 17.6% in AAHP-heated rooms. This indicated that the draught sensation is significantly weaker in AAHP-heated rooms after defrosting operation.

Fig. 9 depicts the variation of thermal sensation votes (TSVs) for subjects before and after the defrosting process. Owing to the decrease in indoor temperature and the increase in draught sensation as displayed in Figs. 7-8, the TSV decreased significantly after defrosting. Consequently, in all rooms, the TSV of subjects exhibits a typical W-shaped variation pattern throughout the continuous frosting-defrosting processes. Detailed change degrees of subjects' thermal sensation after defrosting operation are illustrated in Fig. 10. In AWHP-heated rooms, 78.4% of the subjects reported a downgrade in thermal sensation after defrosting, with 42.1% indicating a one-level decrease, 30.4% indicating a two-level decrease, and 5.9% indicating a three-level decrease. In contrast, in AAHP-heated rooms, 73.5% of the subjects perceived a decline in thermal sensation, among whom 61.8% and 11.7% experienced one- and two-level decreases, respectively, while no subject reported a three-level decrease.

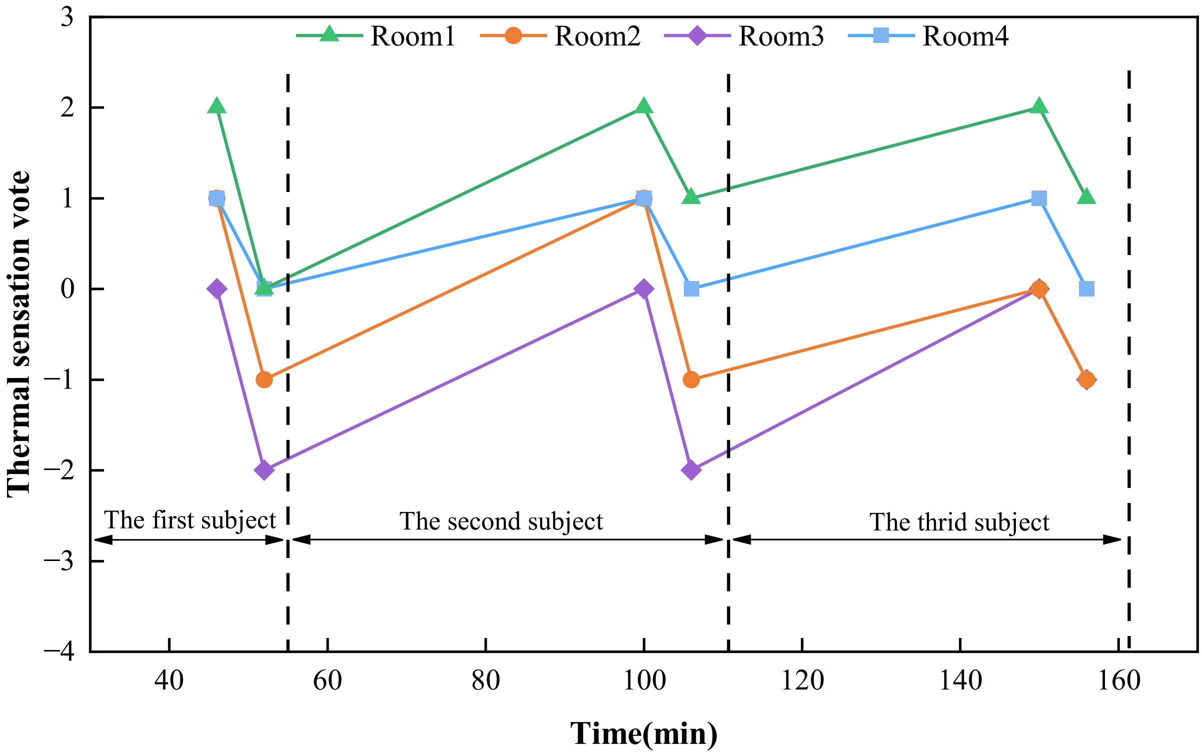

Fig.9 Variation trend of thermal sensation vote values for subjects during defrosting process

These results indicated that the thermal sensation of the subjects decreased significantly after the defrosting operation for both the AWHP and the AAHP. However, in AAHP-heated rooms , owing to the weaker draught sensation (Fig. 8) as well as smaller fluctuation duration and fluctuation range of indoor temperature (Fig. 7), the thermal sensation primarily decreased by only one level, whereas in AWHP-heated rooms, the thermal sensation tended to decrease by one or two levels. Therefore, the defrosting operation of the AWHP had a greater negative impact on the thermal sensation of the subjects than that of AAHP.

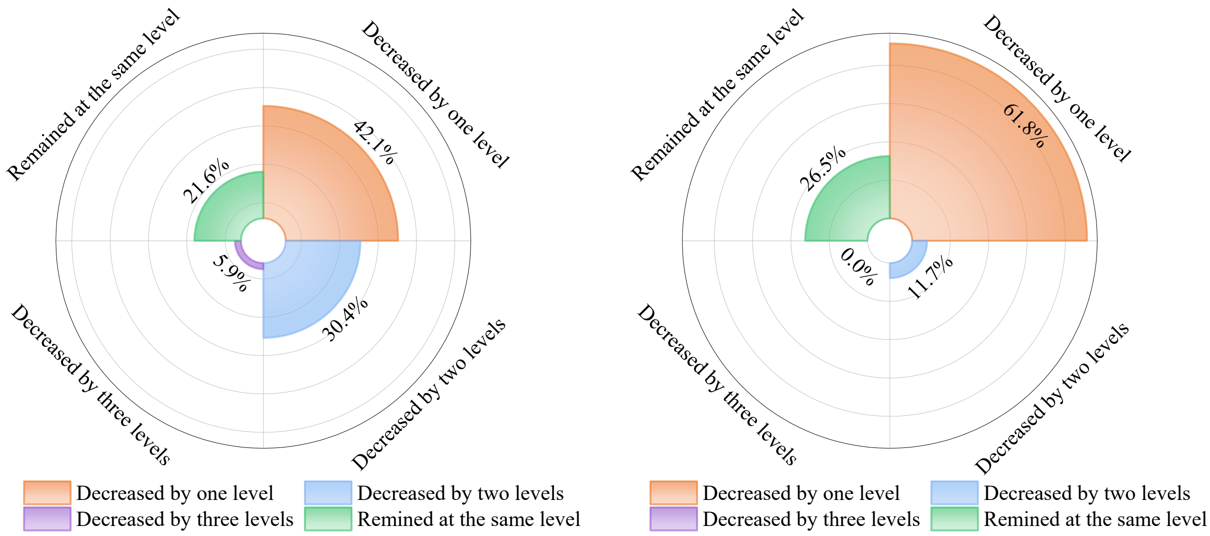

(a) Air-water heat pump (b) Air-air heat pump

Fig.10 Degree of change in subjects' thermal sensation after ASHP defrosting

Fig. 11 presents the variations in human thermal acceptability before and after the defrosting operation of the AWHP and AAHP. Before the defrosting operation of AWHP, 5.9% of subjects believed that the environment was "clearly acceptable", and 81.4% of subjects believed it was "just acceptable", accounting for 87.3% of all subjects. In contrast, only 6.9% and 5.8% of the subjects respectively considered the environment to be "just unacceptable" and "clearly unacceptable". After defrosting, the proportions changed significantly, with 41.1% and 47.1% of subjects rating the environment as "clearly unacceptable" and "just unacceptable", respectively. Only 11.8% of the subjects regarded it as "just acceptable", while none rated it as “clearly acceptable”. This indicated that the acceptance rate for the indoor thermal environment (i.e., those who reported “clearly acceptable” or “just acceptable”) dropped sharply from 87.3% before defrosting to 11.8% after defrosting in the AWHP-heated rooms.

For the AAHP-heated room, before defrosting, 26.5%, 61.8%, 11.7%, and 0 of the subjects reported the indoor thermal environment as “clearly acceptable”, “just acceptable”, “just unacceptable”, and “clearly unacceptable”, respectively. The acceptance rate reached 88.3%. After defrosting, these proportions changed to 11.8%, 26.4%, 55.9%, and 5.9%, respectively, with the acceptance rate declining markedly to 38.2%. This indicated that acceptance rate for the indoor thermal environment dropped significantly from 88.3% before defrosting to 38.2% after defrosting in the AWHP-heated rooms.

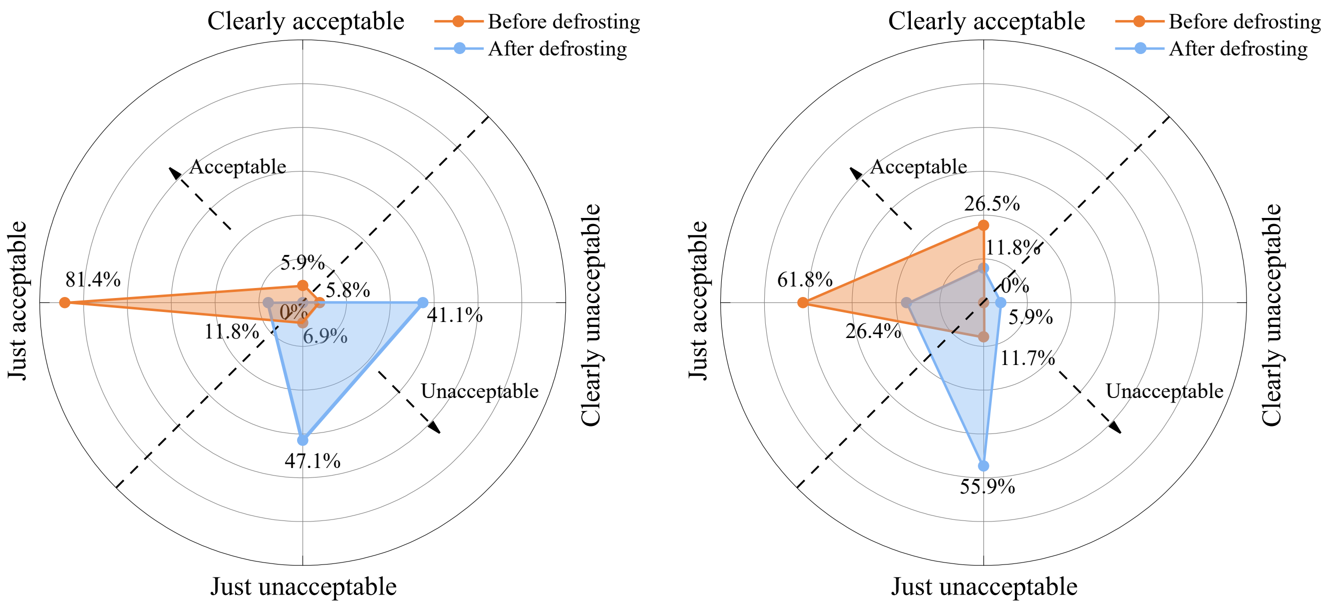

(a)Air-water heat pump (b)Air-air heat pump

Fig.11 subjects’ acceptability votes before and after ASHP defrosting

The above results showed that before defrosting, the proportion of subjects who rated the thermal environment acceptable was similar in the AWHP-heated rooms and AAHP, at 87.3% and 88.3%, respectively. However, after defrosting, the proportion of subjects who rated the thermal environment acceptable dropped significantly, to 11.8% and 38.2%, respectively. This indicated that after defrosting, the proportion of subjects satisfied with the thermal environment in the AAHP-heated room was significantly greater than that in the AWHP-heated rooms. Therefore, compared to AAHP, the defrosting operation of AWHP has a greater impact on the indoor thermal environment.

3.3 Subjective preferences for subjects

In addition to the above subjective thermal comfort indicators, the questionnaire also collected the subjective preferences of subjects, specifically including thermal expectation, humidity expectation, draught sensation expectation, and overall satisfaction. Fig. 12(a) and Fig. 12(b) present the distribution of subjects' thermal expectations before and after the defrosting operation for both AWHP and AAHP systems. For AWHP-heated rooms, 68.6% of the subjects expected the thermal condition to remain unchanged before defrosting, while only 19.6% preferred an increased thermal condition, as displayed in Fig. 12(a). After defrosting, owing to the significant decline in indoor temperature (Fig. 7(a)) and the increased draught sensation (Fig. 8), the proportion of subjects preferring an increased thermal condition rose to 81.4%, whereas only 12.7% still preferred unchanged conditions. Fig.12(b) illustrates the change of thermal expectations in AAHP-heated rooms. The proportion of subjects expected the thermal condition to remain unchanged fell from 70.6% before defrosting to 38.2% after defrosting, while that desiring an increased thermal condition increased from 5.9% to 61.8%. This demonstrates that in rooms heated by AWHP and AAHP, the variation trends of thermal expectation after defrosting operation were same. Specifically, the percentages of subjects who expected the thermal condition to "remain unchanged" and "decreased" decreased, while that expected the thermal condition to "increased" rose significantly. Nevertheless, the proportion of subjects expecting an increased thermal condition after defrosting was substantially greater for the AWHP-heated rooms (81.4%), compared to that in AAHP-heated rooms (61.8%). This indicates that the defrosting operation of AWHP has a greater impact on indoor thermal comfort.

Fig. 12(c) and Fig. 12(d) illustrate the distribution of subjects' humidity expectations before and after defrosting for both AWHP and AAHP systems. In AWHP-heated rooms, the proportion of subjects preferring to maintain the current humidity increased from 64.7% to 70.6%, while those expecting higher humidity decreased from 35.3% to 29.4%. Similarly, in the AAHP-heated room, the proportion of subjects favoring the current condition rose from 82.4% to 88.2%, whereas those desiring higher humidity declined from 17.6% to 11.8%.

Due to the increase in indoor relative humidity after defrosting (Fig. 7), the demand for higher humidity decreased, while satisfaction with the existing humidity level increased. As the indoor relative humidity remained consistently low throughout the frosting-defrosting processes, none of the subjects expressed a preference for lower humidity.

Fig. 12(e) and Fig. 12(f) illustrate the distribution of subjects' draught sensation expectations for before and after the defrosting operation for both the AWHP and AAHP systems. In AWHP-heated rooms, a pronounced draught sensation was observed after defrosting, as shown in Fig. 8(a). Consequently, the proportion of subjects expecting the draught sensation to remain unchanged decreased sharply, from 58.8% before defrosting to 18.6% afterward. Correspondingly, the proportion of subjects expecting a decrease in draught sensation increased markedly, rising from 36.3% to 81.4%. In contrast, in AAHP-heated rooms, where the draught sensation after defrosting remained essentially unchanged, as shown in Fig. 8(b), the proportion of subjects expecting a decrease in draught sensation increased slightly, from 20.6% to 29.4%, representing a modest growth of 8.8%.

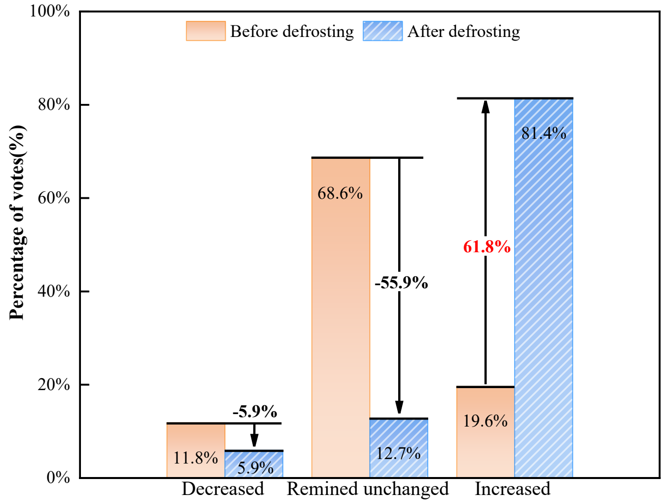

(a) Thermal expectations for AWHP

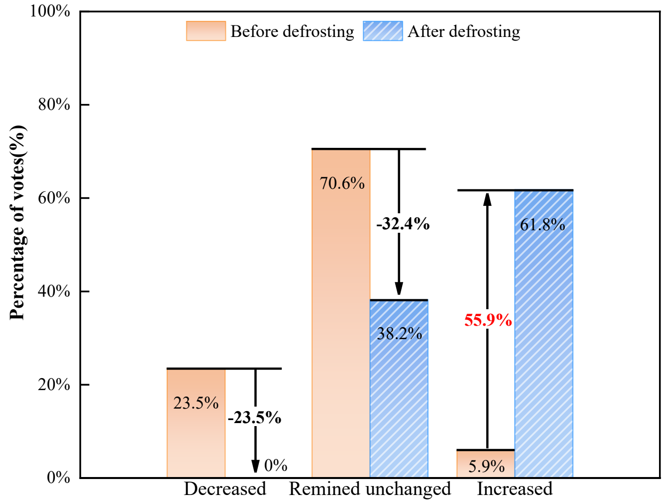

(b) Thermal expectations for AAHP

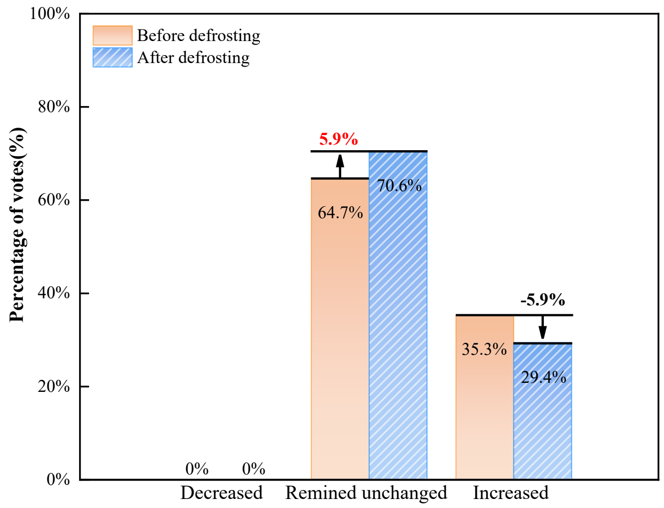

(c) Humidity expectations for AWHP

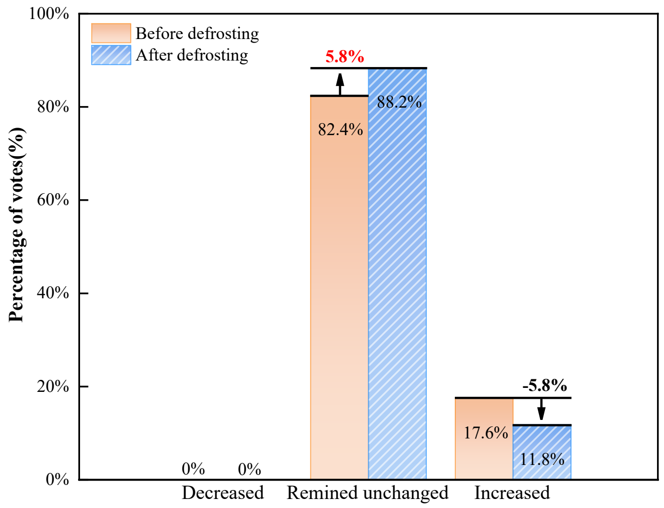

(d) Humidity expectations for AAHP

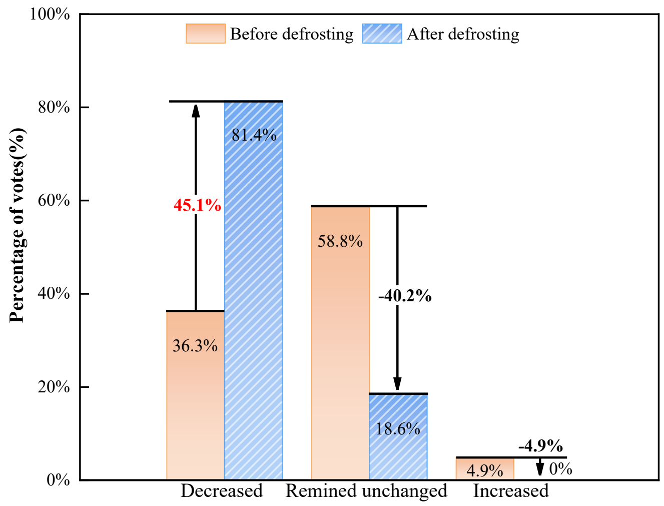

(e) Draught expectations for AWHP

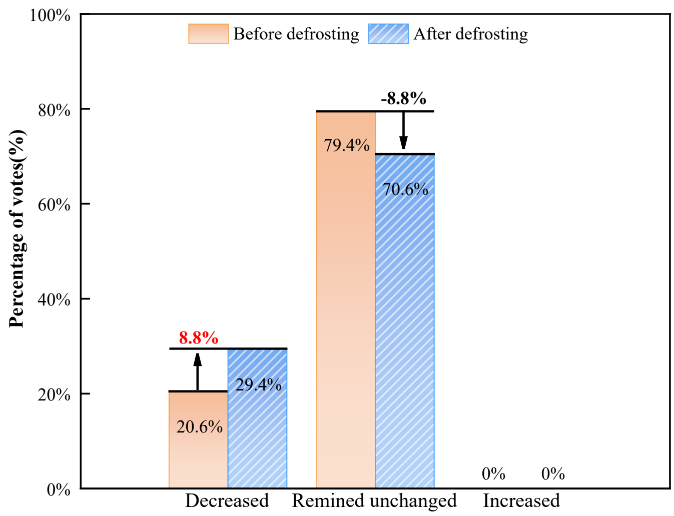

(f) Draught expectations for AAHP

Fig. 12 Change in expectations before and after defrosting

Overall, compared with the AAHP, the AWHP results in a significantly higher proportion of subjects expecting a reduction in draught sensation after defrosting. This underscores the urgent need to develop control strategies for the indoor fan coils of AWHPs to mitigate draught discomfort following defrosting.

Fig. 13 shows the overall satisfaction of subjects before and after defrosting operation for both AWHP and AAHP. In AWHP-heated rooms, 75.5% of subjects reported satisfaction before defrosting, including 70.6% being "just satisfied" and 4.9% being "clearly satisfied," while 24.5% expressed dissatisfaction. After defrosting, the dissatisfaction rate sharply increased to 71.6%, representing a relative rise of 192.2%. In AAHP-heated room, 79.4% of subjects were satisfied before defrosting (64.7% "just satisfied" and 14.7% "clearly satisfied"), whereas 20.6% were dissatisfied. After defrosting, the dissatisfaction rate increased to 64.7%, corresponding to a relative increase of 214%. Notably, the distributions of dissatisfaction responses varied obviously for the two systems. In AWHP-heated rooms, the "clearly dissatisfied" responses predominated (47.1%), whereas in AAHP-heated room, "just dissatisfied" responses accounted for the largest proportion (41.2%).

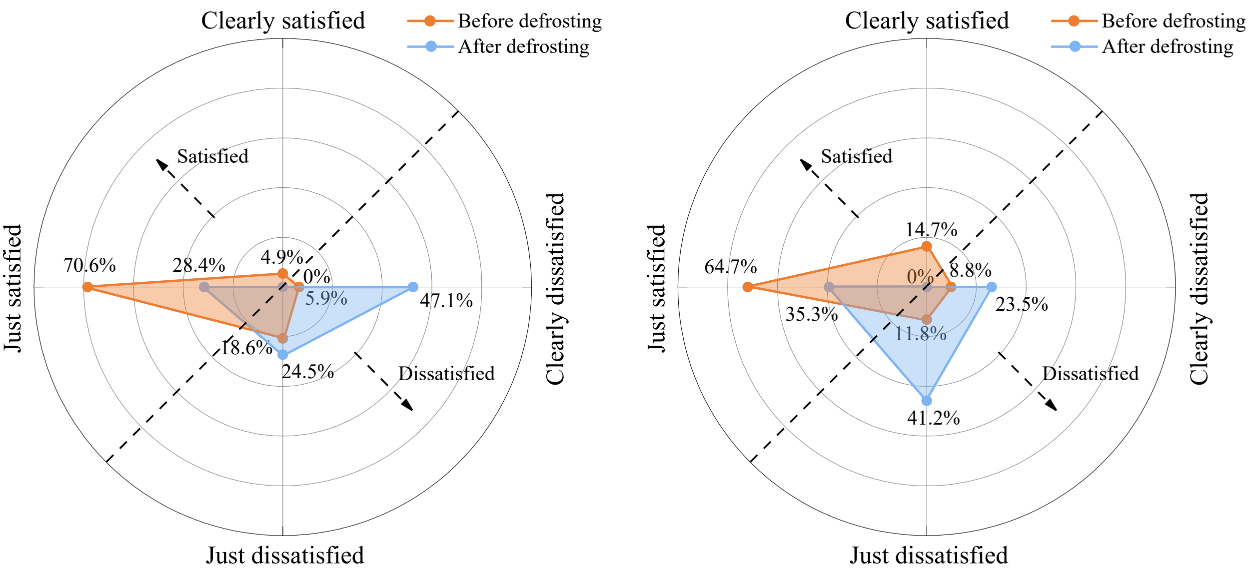

(a) Air-water heat pump (b) Air-air heat pump

Fig.13 Overall satisfaction of subjects before and after ASHP defrosting

3.4 Thermal acceptability of indoor temperature at the beginning of defrosting

Through the discussion above, it can be obtained that the indoor thermal comfort decreases obviously after defrosting. To improve the thermal comfort during the whole frosting-defrosting process, the influence factors on the indoor thermal comfort were analyzed, and it was found the key influence factor was the indoor temperature range at the end of defrosting. However, the indoor temperature at this point is uncontrollable. To solve this issue, the indoor temperature variations in the all rooms during frosting-defrosting process were analyzed. As displayed in Fig. 7, the indoor temperature at the end of defrosting was positively correlate with that at the beginning of defrosting. As the indoor temperature at the beginning of defrosting was controllable, the relationship between this temperature and the mean TSV at the end of defrosting was investigated, and used to improve the thermal comfort during the whole frosting-defrosting process.

Fig. 14 illustrates the relationship between mean TSV of subjects and indoor temperature in the AWHP-heated rooms and AAHP. As expressed in Section 2.2, the setting values of indoor temperature were 20±3 °C, 22±3 °C, 24±3 °C and 22±3 °C in turn. The theoretical variation range of indoor temperature in AWHP-heated rooms was 17-27 °C, while 19-25 °C in AAHP-heated rooms. However, during the experimental process of AWHP, the measured indoor temperature at the beginning of defrosting was 17.5-26 °C. Therefore, the indoor temperature ranges of the two types of ASHPs were 17.5-26 °C and 19-25 °C. For both the two types of ASHPs, the mean TSV increased with the indoor temperature overall. The equations between the mean TSV and indoor temperature were fitted as displayed in Eqs. (3) and (4). The values of R^2 for the two fitting equations were 0.946 and 0.937. When the TSV was equal to 0, the thermal neutral temperature could be obtained. For the AWHP-heated rooms and AAHP, it was 22.91 °C and 22.18 °C, respectively.

When the TSV falls in the range of -1 to 1, it is thought that the indoor temperature is acceptable for subjects [43, 44]. For the AWHP-heated rooms, when the TSV was equal to -1 and 1, the corresponding indoor temperatures were 20.74 °C and 25.09 °C, as demonstrated in Fig. 14(a). Meanwhile, for the AAHP-heated rooms, the corresponding indoor temperatures were 19.91 °C and 24.45 °C, as displayed in Fig. 14(b). Consequently, the acceptable indoor temperature at the beginning time of defrosting was obtained, and it was 20.74-25.09 °C for AWHP-heated rooms and 19.91-24.45 °C for AAHP-heated rooms. Compared to those heated by AAHP, the indoor temperature at the beginning time of defrosting for AWHP-heated rooms should be 0.64-0.83 °C higher.

$$TSV = 0.46T_{in} - 10.54 \tag{3}$$

$$TSV = 0.44T_{in} - 9.76 \tag{4}$$

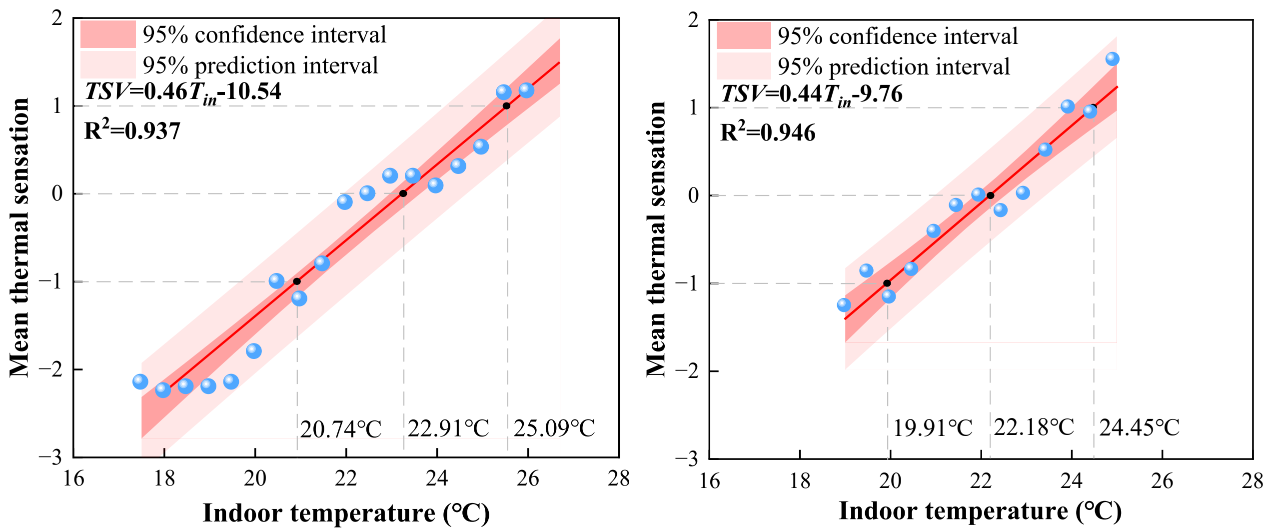

(a) Air-water heat pump (b) Air-air heat pump

Fig.14 The relationship between the mean thermal sensation vote and indoor temperature after ASHP defrosting

4 Conclusions

To improve the indoor thermal comfort during the frosting-defrosting process of ASHP, two test rigs, an AWHP heating system and an AAHP heating system, were built up in an artificial climate chamber. Through creating a stable frosting environment, the sensations of subjects during frosting-defrosting process were analyzed through a questionnaire survey. At last, the thermal acceptability of indoor temperature at the beginning of defrosting was investigated. The findings are summarized below.

(1) In rooms heated by both AWHP and AAHP, the indoor temperature during defrosting process decreased obviously, and the descend range in former was greater. During the defrosting process, the indoor temperature in AWHP-heated rooms decreased 2.6-4.6 ℃, while it decreased 1.4-1.9 ℃ in AAHP-heated rooms. The descend range of indoor temperature in AAHP-heated rooms was obvious lower than that in AWHP-heated rooms.

(2) After defrosting, the thermal sensation of subjects in AWHP-heated rooms and AAHP both decreased significantly. For the AWHP-heated rooms, the thermal sensation of 78.4% subjects decreased after defrosting, including 42.1% experiencing a decrease of one level, 30.4% experiencing a decrease of two levels, and 5.9% experiencing a decrease of three levels. Meanwhile, for the AAHP-heated rooms, the thermal sensation of 73.5% subjects decreased after defrosting, including 61.8% experiencing a decrease of one level, 11.7% experiencing a decrease of two levels.

(3) After defrosting, the warmer thermal environment and weaker draught sensation were expected by most subjects. The ratio of subjects expecting a warmer environment in AWHP-heated rooms increased from 19.6% before defrosting to 81.4% after defrosting, while from 5.9% before defrosting to 61.8% after defrosting in the AAHP-heated rooms. Meanwhile, the ratio of subjects expecting a weaker draught sensation in AWHP-heated rooms increased from 36.3% to 81.4%, while only from 20.6% to 29.4% in AAHP-heated rooms. This indicated it is urgent to develop a better control strategy for the indoor fan coils of AWHP during defrosting.

(4) The acceptable indoor temperatures at the beginning time of defrosting for AWHP-heated rooms and AAHP were obtained. According to the relationship between TSV and indoor temperature at the

beginning time of defrosting, the acceptable indoor temperature at the beginning time of defrosting was 20.74-25.09 °C for the AWHP-heated rooms, and 19.91-24.45 °C for the AAHP-heated rooms. Compared to those heated by AAHP, the indoor temperature at the beginning time of defrosting for AWHP-heated rooms should be 0.64-0.83 °C higher.

Acknowledgements

This work was financially supported by the National Natural Science Foundation of China (No. 52408098) and the National Support Program for Young Talent in Built Environment and Energy Engineering (2025-2027).

References

[1] A. Zhang, F. Wang, H. Li, B. Pang, K. Nie, X. Ma, C. Zhuang, Z. Pan, Y. Jiang, J. Yang, A framework of carbon-negative rural housing renovation with novel heating methods and digital twin-based carbon emission monitoring, Building and Environment 282 (2025) 113158.

[2] Y. Yang, R. Adhikari, Y. Lou, J. O'Donnell, N. Hewitt, W. Zuo, Long-term impact of electrification and retrofits of the U.S residential building in diverse locations, Building and Environment 269 (2025) 112472.

[3] Y. Chen, M. Quan, D. Wang, Z. Tian, Z. Zhuang, Y. Liu, E. He, Energy, exergy, and economic analysis of a solar photovoltaic and photothermal hybrid energy supply system for residential buildings, Building and Environment 243 (2023) 110654.

[4] Q.L. Han, D.Y. Jiang, S.J. Chen, Y. Fu, H.M. Duan, Molecular insights into the influence of synergistic effect on adsorption-hydration hybrid CH4 storage in ZIF-8@AC composite materials, Journal of Materials Chemistry A 13(33) (2025) 27493-27503.

[5] S. Sangsinsorn, B. Nienborg, Noise immissions by air source heat pumps: A case study in Germany, Building and Environment 279 (2025) 113037

[6] Y. Tan, W.Z. Wei, W. Wang, Y.Y. Sun, S.Q. Wang, Z.K. Li, Z.Y. Li, R. Tang, C.X. Zhang, S. Wei, Experimental and theoretical research on evaluation criterion for defrosting initiation time accuracy of air source heat pump, Applied Thermal Engineering 278 (2025).

[7] L. Zhang, Y. Jiang, J. Dong, Y. Yao, S. Deng, An experimental study of frost distribution and growth on finned tube heat exchangers used in air source heat pump units, Applied Thermal Engineering 132 (2018) 38-51.

[8] W. Wang, Y. Tan, W.Z. Wei, Y.Y. Sun, S.L. Han, C.M. Dai, A performance prediction model of variable frequency air source heat pump used for photovoltaic power generation scheduling in low-carbon buildings, Renewable Energy 238 (2025).

[9] S. Huang, H. Yu, M. Zhang, H. Qu, L. Wang, C. Zhang, Y. Yuan, X. Zhang, Advances, challenges and outlooks in frost-free air-source heat pumps: A comprehensive review from materials, components to systems, Applied Thermal Engineering 234 (2023) 121163.

[10] T. Xiong, H. Wu, L.X. Hu, G.Q. Liu, G. Yan, Optimal design of vapor-bypassed heat exchanger for performance improvement of air source heat pump system, Renewable Energy 249 (2025).

[11] W. Wang, H. Di, R. Tang, W. Wei, Y. Sun, C. Dai, Effect of supply water temperature on frosting performance of air source heat pump and indoor thermal environment in space heating, Building and Environment 267 (2025) 112258.

[12] T. Xiong, L. Hu, G. Liu, G. Yan, Transient refrigerant distribution in a microchannel heat exchanger heat pump system under different reverse cycle defrosting strategies, Case Studies in Thermal Engineering 61 (2024) 105069.

[13] P. Jiang, Y. Zhang, H. Fan, Q. Jin, Y. Yu, Experimental study of solution defrosting characteristics of air source heat pump, Applied Thermal Engineering 236 (2024) 121575.

[14] W. Wang, Y.C. Feng, J.H. Zhu, L.T. Li, Q.C. Guo, W.P. Lu, Performances of air source heat pump system for a kind of mal-defrost phenomenon appearing in moderate climate conditions, Applied Energy 112 (2013) 1138-1145.

[15] Y. Wu, W. Wang, Y. Sun, Y. Cui, Y. Lin, S. Deng, Development of evaluation indexes for assessing the regional operating performances of air source heat pump (ASHP) units operated in different climate regions based on the equivalent temperature drop method, Energy and Buildings 247 (2021) 111111.

[16] X. Li, G. Ma, T. Lu, L. Gao, W. Rong, Y. Gong, S. Xu, Experimental study on defrosting multi outdoor units in turn for air source heat pump using hot gas, International Journal of Refrigeration 174 (2025) 76-85.

[17] J. Ma, D. Kim, J.E. Braun, W.T. Horton, Development and validation of a dynamic modeling framework for air-source heat pumps under cycling of frosting and reverse-cycle defrosting, Energy 272 (2023) 127030.

[18] W. Wei, B. Wang, H. Gu, L. Ni, Y. Yao, Investigation on the regulating methods of air source heat pump system used for district heating: Considering the energy loss caused by frosting and on-off, Energy and Buildings 235 (2021) 110731.

[19] Z. Yang, M. Cui, H. Xiao, H. Sun, B. Wang, B. Lin, W. Shi, Analysis of thermal comfort experience using peak-end rule with air conditioner in heating season, Building and Environment 229 (2023) 109965.

[20] N. Lyu, Z. Shao, H. He, F. Wang, C. Liang, X. Zhang, Performance study of an active-passive combined anti-frosting method for fin-tube heat exchanger, Building and Environment 222 (2022) 109365.

[21] W.M. Yan, H.Y. Li, Y.J. Wu, J.Y. Lin, W.R. Chang, Performance of finned tube heat exchangers operating under frosting conditions, International Journal of Heat and Mass Transfer 46(5) (2003) 871-877.

[22] M. Song, C. Dang, M. Ning, S. Deng, Energy transfer procession in an air source heat pump unit during defrosting with melted frost locally drainage in its multi-circuit outdoor coil, Energy and Buildings 164 (2018) 109-120.

[23] S. Wang, W. Wei, W. Wang, Y. Sun, Z. Li, C. Dai, C. Huang, R. Tang, S. Deng, Frosting-defrosting performance variations of air source heat pumps with the type of refrigerants: R410A and R32 as an example, Applied Thermal Engineering 262 (2025) 125189.

[24] Z. Li, Y. Sun, W. Wang, W. Wei, An improved equivalent temperature drop method for evaluating the operating performances of ASHP units under frosting conditions considering their configuration and operation, Energy and Buildings 331 (2025) 115370.

[25] Y. Lin, W. Wang, J. Luo, Y. Sun, S. Deng, A novel variable speed ASHP frosting suppression operation method based on the frosting suppression performance map, Applied Thermal Engineering 234 (2023) 121254.

[26] Z. Zhou, G. Li, H. Chen, H. Zhong, Fault diagnosis method for building VRF system based on convolutional neural network: Considering system defrosting process and sensor fault coupling, Building and Environment 195 (2021) 107775.
[27] H. Bai, P. Liu, H.M. Mathisen, Evaluation of frost prevention strategies for membrane energy exchangers, Building and Environment 244 (2023) 110814.
[28] D.L. da Silva, C.J.L. Hermes, Optimal defrost cycle for air coolers revisited: A study of fan-supplied tube-fin evaporators, International Journal of Refrigeration-Revue Internationale Du Froid 89 (2018) 142-148.
[29] W. Wang, S. Zhang, Z. Li, Y. Sun, S. Deng, X. Wu, Determination of the optimal defrosting initiating time point for an ASHP unit based on the minimum loss coefficient in the nominal output heating energy, Energy 191 (2020) 116505.
[30] Z. Li, W. Wang, Y. Sun, S. Wang, S. Deng, Y. Lin, Applying image recognition to frost built-up detection in air source heat pumps, Energy 233 (2021) 121004.
[31] R. Tang, W. Wei, P. Sun, J. Zhao, W. Wang, Y. Sun, S. Deng, A novel time-current-temperature difference (T-I-T) defrosting control method for air source heat pump based on outdoor fan operation characteristics in space heating, Applied Thermal Engineering 259 (2025) 124850.
[32] W. Wei, C. Wu, L. Ni, W. Wang, Z. Han, W. Zou, Y. Yao, Performance optimization of space heating using variable water flow air source heat pumps as heating source: Adopting new control methods for water pumps, Energy and Buildings 255 (2022) 111654.
[33] M. Qu, T. Li, S. Deng, Y. Fan, Z. Li, Improving defrosting performance of cascade air source heat pump using thermal energy storage based reverse cycle defrosting method, Applied Thermal Engineering 121 (2017) 728-736.
[34] S. Liu, X. Bai, S. Deng, L. Zhang, M. Wei, Developing a novel control strategy for frosting suppression based on condensing-frosting performance maps for variable speed air source heat pumps, Energy and Buildings 289 (2023) 113049.
[35] M. Qu, L. Xia, S. Deng, Y. Jiang, Improved indoor thermal comfort during defrost with a novel reverse-cycle defrosting method for air source heat pumps, Building and Environment 45(11) (2010) 2354-2361.
[36] N. Mao, H. Yu, T. He, Y. Xu, Unsteady characteristics of sleeping thermal comfort during defrosting of a T-ASHP system, Indoor and Built Environment 31(6) (2022) 1715-1729.
[37] W. Wei, L. Ni, W. Wang, Y. Yao, Experimental and theoretical investigation on defrosting characteristics of a multi-split air source heat pump with vapor injection, Energy and Buildings 217 (2020) 109938.
[38] Z. Li, W. Wei, W. Wang, Y. Sun, S. Wang, R. Tang, Y. Lin, C. Huang, S. Deng, Determination of the defrosting duration ratio for defrosting performance evaluation of air source heat pump, Journal of Building Engineering 95 (2024) 110305.
[39] Standards Press of China, Beijing, GB/T 25127.1-2020, Low Ambient Temperature Air Source Heat Pump (Water Chilling) Packages Part 1: Heat Pump (Water Chilling) Packages for Industrial & Commercial and Similar Application, 2020.
[40] Air Conditioning Heating and Refrigeration Institute, ANSI/AHRI Standard 550/590-2023 (I-P), Performance Rating of Water-Chilling and Heat Pump Water-Heating Packages Using the Vapor Compression Cycle, Air Conditioning Heating and Refrigeration Institute, 2023.
[41] ANSI/ASHRAE Standard 55-2004, Thermal Environmental Conditions for Human Occupancy, American Society of Heating, Refrigeration and Air-conditioning Engineers, Inc., 2004.

[42] International Organization for Standardization, ISO7730:2005, Ergonomics of the Thermal Environment — Analytical Determination and Interpretation of Thermal Comfort Using Calculation of the PMV and PPD Indices and Local Thermal Comfort Criteria, 2005.
[43] B. Li, C. Du, R. Yao, W. Yu, V. Costanzo, Indoor thermal environments in Chinese residential buildings responding to the diversity of climates, Applied Thermal Engineering 129 (2018) 693-708.
[44] N. Zhang, B. Cao, Z. Wang, Y. Zhu, B. Lin, A comparison of winter indoor thermal environment and thermal comfort between regions in Europe, North America, and Asia, Building and Environment 117 (2017) 208-217.